# research papers

# X-ray reflectivity measurements of liquid/solid interfaces under high hydrostatic pressure conditions

**Florian J. Wirkert, Michael Paulus, Julia Nase,\* Johannes Möller, Simon Kujawski, Christian Sternemann and Metin Tolan**

Fakultät Physik/DELTA, TU Dortmund, 44221 Dortmund, Germany.
\*E-mail: julia.nase@tu-dortmund.de

A high-pressure cell for *in situ* X-ray reflectivity measurements of liquid/solid interfaces at hydrostatic pressures up to 500 MPa (5 kbar), a pressure regime that is particularly important for the study of protein unfolding, is presented. The original set-up of this hydrostatic high-pressure cell is discussed and its unique properties are demonstrated by the investigation of pressure-induced adsorption of the protein lysozyme onto hydrophobic silicon wafers. The presented results emphasize the enormous potential of X-ray reflectivity studies under high hydrostatic pressure conditions for the *in situ* investigation of adsorption phenomena in biological systems.

## 1. Introduction

Studying the response of matter to pressure has a long tradition, since phase transitions and phase separations can be investigated in great detail. Such transitions are induced by the reduction of the sample volume, which has an impact on, for example, interaction potentials, dynamic degrees of freedom, and bonding. High pressure allows inducing conformational modifications to proteins without bringing internal energy into the system, meaning that volume effects and energy effects can be analyzed separately. The importance of studying biological systems at hydrostatic pressures up to 5 kbar lies also in the fact that biologically relevant proteins denature in this pressure regime.

The use of high pressure (Jayaraman, 1983) in combination with synchrotron-radiation-based small-angle X-ray scattering (Winter, 2002; Liu *et al.*, 2012), X-ray diffraction (Meade *et al.*, 1992; Katrusiak & McMillan, 2004; McMahon, 2012) and X-ray spectroscopy (Ingalls *et al.*, 1980; Ishimatsu *et al.*, 2012; Hong *et al.*, 2013; Jackson *et al.*, 2005; McCammon *et al.*, 2008; Rueff & Shukla, 2010) is well established and provides unique insights into the structure of soft and hard condensed matter. In the past, pressure ranging from kbar to several Mbar was applied in cells that make use of compressed fluids (*e.g.* Pressl *et al.*, 1997; Kato & Fujisawa, 1998; Woenckhaus *et al.*, 2000; Krywka *et al.*, 2008; Ando *et al.*, 2008) or diamond anvils (*e.g.* Loubeyre *et al.*, 1996; Tateno *et al.*, 2010) to pressurize a very small sample volume. However, it is the specific scattering geometry in an X-ray reflectivity (XRR) experiment and thereby the requirements to the sample dimensions that complicate the construction of a high-pressure XRR sample cell. For reflectivity experiments, large samples surfaces are needed because of the very small angles at which the incoming beam hits the sample. At such grazing angles, the beam size on the sample, the so-called footprint, is larger than the sample itself and intensity is lost. Thus, samples with surfaces up to a square centimeter need to be placed into the pressurized volume, restricting the minimum cell volume. In recent years, several high-pressure cells for neutron reflectivity were developed and pressures up to 2.5 kbar were achieved (Kreuzer *et al.*, 2011; Jeworrek *et al.*, 2011; Wang *et al.*, 2012; Carmichael *et al.*, 2012). However, X-ray reflectivity studies at the solid/gas, liquid/gas and liquid/liquid interfaces have been limited to pressures below 0.1 kbar in large-volume gas cells (Paulus *et al.*, 2008; Lehmkühler *et al.*, 2009; Venturini *et al.*, 2011; Boewer *et al.*, 2012) so far.

In this article we present a set-up for *in situ* X-ray reflectivity studies of solid/liquid interfaces at high hydrostatic pressures. We report on the first study of the solid/liquid interface at hydrostatic pressures up to 5 kbar and with an accessible $q_z$-range up to 0.5 Å$^{-1}$. First we describe the high-pressure cell and the corresponding sample environment. Then we discuss first X-ray reflectivity measurements of pressure-induced lysozyme adsorption on hydrophobic silicon wafers to demonstrate the enormous potential of the set-up, particularly for the study of biological systems.

## 2. The high hydrostatic pressure X-ray reflectivity cell

To build a high hydrostatic pressure cell, it is necessary to separate the sample volume from the pressure-transmitting liquid, which is usually water. Thus, a two-cell design has to be

used, with an outer cell for pressure application and an inner cell containing the sample liquid and the solid sample. The pressure coupling between the two cells is realised *via* a flexible membrane. The outer cell has to resist the high pressure and is thus made of high-strength steel (type 2.4668, NiCr19Fe19Nb5Mo3). Its general layout is similar to the one developed by Krywka *et al.* (2008), but was modified to carry the significantly larger inner sample cell. The outer dimensions of this cell are 98 mm × 90 mm × 80 mm (length in beam direction × width × height). It is interspersed by channels for water cooling or heating, so that temperatures between 274 K and 360 K can be achieved. A sketch of the sample cell is shown in Fig. 1(*a*). For beam entry and exit, two 25 mm-deep bore holes with M32 × 1.5–6H threads are made opposite each other (marking W). These two holes are connected by a 26.2 mm-long and 14 mm-wide bore that contains the inner sample cell and is filled with pressure-transmitting medium. This volume is connected to a high-pressure pump (SITEC-Sieber Engineering AG, Switzerland) *via* a 2 mm-wide channel that ends in a M16 × 1.5–6H drill hole on the top side of the cell. The connection to the pressure pump is realised by high-pressure-resistant steel tubing. A second 2 mm-wide channel connects the pressurized volume to a pressure monitor (SITEC-Sieber Engineering AG, Switzerland) that is installed at the back *via* a M16 × 1.5–6H drill hole. The pressurized volume is closed by two cylinders with diamond windows (D). Synthetic diamonds with a thickness of 1 mm and a diameter of 6 mm were used as window material. The cylinders have
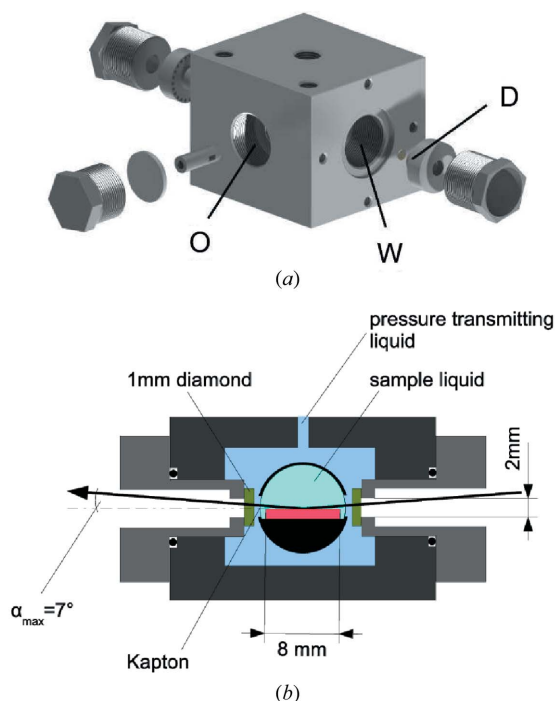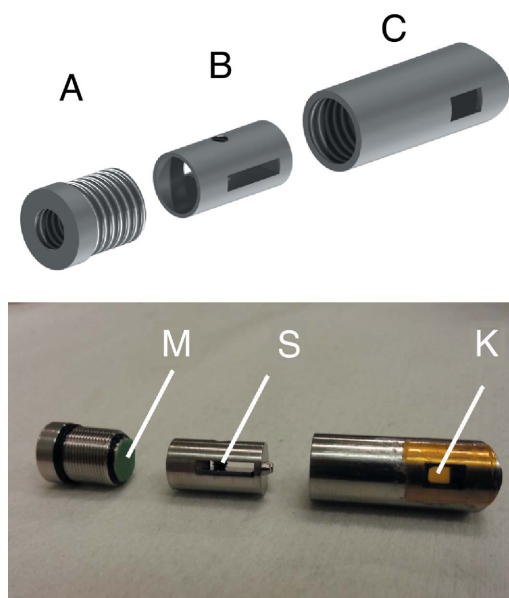
centered circular windows with a diameter of 2 mm, closed by gluing the diamond windows onto the cylinders. O-ring seals are clamped between the cylinders and the cell body to tighten the cell. The seals and cylinders are fixed by the hollow-bored M32 screws (steel type 1.6580, 30CrNiMo8). To reduce the strong absorption of both the diamond windows and the liquid, high photon energies $\geq 20$ keV are required (Paulus *et al.*, 2008). The arrangement of the diamond windows allows a maximum angle of incidence of $\alpha = 7.7°$ at a beam height of 0.1 mm. Typical reflectivity curves of solid/water interfaces can only be measured up to a maximum wavevector transfer $q_{max}$ of approximately 1 Å$^{-1}$ because the signal is too weak at higher $q_z$ (see, for example, Mezger *et al.*, 2006). Thus, the opening angle of our cell is sufficient to measure a complete reflectivity curve without cutting intensity at the window edges.

An additional M32 × 1.5–6H hole (O) is made in the side wall. This opening allows the inner sample cell to be inserted from the side into the outer cell without removing the diamond windows.

The key part of the set-up is the inner sample cell, shown in Fig. 2, which consists of parts *A*, *B* and *C*. It is made of stainless steel. Part *B* is the actual sample holder. The inner volume of this cell including the sample holder is about 375 µl. Two Kapton windows (K in Fig. 2) close the windows in part *C* and separate the liquid sample from the pressure medium, allowing at the same time the beam to enter and exit without intensity loss. The sample holder can accommodate wafers with an area of 8 mm × 8 mm, sufficiently large to carry out X-ray reflectivity measurements. An M3 grub screw (S in Fig. 2) prevents the samples from shifting, which is important



**Figure 1**
(*a*) Sketch of the sample cell. Two cylinders (D) hold the diamond windows, and two M32 screws assure the leak tightness of the cell. The inner cell can be exchanged *via* an opening on the side (O) without removing the diamond windows. (*b*) Schematic drawing of the scattering geometry.



**Figure 2**
Drawing and photograph of the inner sample cell, consisting of parts *A*, *B* and *C*. Part *B* is the actual sample holder. A window in the breech (part *A*) covered by a rubber membrane (M) compensates the volume and pressure changes. An M3 grub screw (S) is used to fix the sample.

as soon as the wafer is placed in a liquid environment. The volume of the inner cell is separated from the outer volume by a breech (part *A*, Fig. 2). A window within the breech is covered by a rubber membrane (M in Fig. 2). Because of its flexibility and elasticity, the rubber membrane provides for the pressure and volume compensations that are necessary because the sample liquid might undergo a pressure-induced volume change. In that way, the collapse of the Kapton windows is prevented. Two bolts at the back of the sample holder *B* fit into appropriate drill holes inside part *C* of the inner cell, thus ensuring the correct orientation of the sample holder with respect to the incident X-ray beam. In order to simplify the insertion of the inner cell into the pressure cell, the rear panel of the inner cell *C* has a concave cylindrical shape, which fits into the corresponding convex structure milled in the pressure cell. In that way, the sample remains stable when the large outer screw in O is fixed. Fig. 1(*b*) shows the beam path in the cell. In total, the X-ray beam passes the two diamond windows (1 mm each), two Kapton windows of the inner cell (25 μm each), approximately 10 mm of sample liquid and approximately 200 μm of water (pressure-transmitting fluid).

With the described set-up, very high hydrostatic pressures up to 5 kbar can be reached. The temperature is stable within ±0.1 K. The pressure loss in the worst case is ∼100 bar during a reflectivity measurement, corresponding to a pressure stability of ±1% at 5 kbar. However, in the best case, the pressure loss can be as small as 10 bar (±0.1%) at higher pressures, and even below that at 1–2 kbar.

## 3. Experiment

In an X-ray reflectivity experiment, the specularly reflected intensity is monitored as a function of the incident angle $\alpha$, see Fig. 1(*b*). The laterally averaged electron density profile $\rho_e(z)$ perpendicular to the sample surface is investigated; $z$ is the vertical distance above the interface. Depending on the set-up and the maximum accessible wavevector transfer $q_z = 4\pi/\lambda \sin(\alpha)$, with the wavelength $\lambda$ of the X-ray radiation, ångstrom resolution is reached. The reflected intensity $I$ is given by (Als-Nielsen & McMorrow, 2001)

$$I(q_z) \propto \frac{1}{q_z^4} \left| \int \frac{\partial \rho_e(z)}{\partial z} \exp(iq_z z) \, dz \right|^2. \quad (1)$$

Thus, the X-ray reflectivity technique provides direct access to the structure of interfaces, averaged over the illuminated area. Notably, structural changes due to adsorption at the solid/liquid interface can be investigated. In a given experimental set-up, the resolution of the electron density profiles is proportional to $1/q_{max}$. Thus, a large $q_z$-range is especially important in the case of very thin layers, where a high resolution is required.

To demonstrate the possibilities that the high-pressure X-ray reflectivity cell offers, we performed a study on pressure-induced adsorption of lysozyme onto hydrophobic surfaces. Lysozyme is an ellipsoid with dimensions of ∼45 Å ×

30 Å × 30 Å. It has a well known structure and has been intensely used as a model protein in many studies so far. The experiments were performed at beamline BL9 (Krywka *et al.*, 2006, 2007) of the synchrotron lightsource DELTA (Dortmund, Germany; see Tolan *et al.*, 2003) using the 27 keV X-ray reflectivity set-up (Paulus *et al.*, 2008).

In the past, the adsorption of lysozyme on hydrophilic and hydrophobic surfaces was studied by X-ray reflectivity experiments under ambient pressure conditions varying different parameters such as protein concentration, pH value, co-solvents or temperature [see, for example, Hähl *et al.* (2012) or Richter & Kuzmenko (2013)]. It was shown that the protein predominantly adsorbs as a monolayer. However, if the temperature was raised to a value where lysozyme starts to unfold, a strong increase of the adsorption occurred (see Jackler *et al.*, 2002). As high pressure also possesses a destabilizing effect on lysozyme; a similar behavior is expected when the pressure is raised. Koo *et al.* (2013) studied the pressure-induced adsorption of lysozyme at the solid/liquid interface applying neutron reflectivity for pressures up to 2 kbar, but in a very limited $q_z$-range of 0–0.1 Å$^{-1}$, indicating a slightly increased lysozyme adsorption.

In this study, lysozyme (14.3 kDa, pI = 11, from hen egg-white, Sigma Aldrich) was used in 25 m$M$ bis-tris buffer solution at pH 7 (Neuman *et al.*, 1973). Because of the high stability of lysozyme, unfolding is expected at pressures above 4 kbar (Schroer *et al.*, 2011). To decrease the unfolding pressure, guanidinium chloride (CH$_6$ClN$_3$; Merck, Darmstadt, Germany), which is known as a protein denaturant (Schellman, 2002), was added with a concentration of 1 $M$ l$^{-1}$. The protein concentration was 0.1 mg ml$^{-1}$. A self-assembled monolayer of octadecyltrichlorosilane (OTS) was prepared on the silica surface of silicon wafers in order to produce a highly hydrophobic surface (Mezger *et al.*, 2006). The wafers were cut into 8 mm × 8 mm pieces and fixed inside the inner cell. Afterwards, the inner-cell volume was filled with a protein–guanidinium-chloride solution and then placed into the high-pressure outer cell. The temperature was set to 313 K.

The incoming X-ray beam ($E_{Ph}$ = 27 keV) had a vertical size of 0.1 mm and a width of 1 mm. The reflected beam was detected by a NaI point detector. The background scattering originated mainly from the bulk scattering of the water phase and was of the order of 10$^{-7}$. It was measured with a longitudinal offset scan. A reflectivity scan including the measurement of the diffusely scattered radiation took 40 min. The $q_z$-range of up to 0.5 Å$^{-1}$ was probed. We expect that at other synchrotron sources, with a flux that is several orders of magnitude above the flux at BL9 of DELTA, the accessible range can be considerably extended.

First, a reference reflectivity at a pressure of 1 bar was recorded before the pressure was raised to 5 kbar. The diffusely scattered radiation was subtracted from the X-ray reflectivity signal. By repeated measurements, it was excluded that radiation damage was at the origin of any observed effects.

Background-corrected reflectivities at ambient (circles) and high pressure (stars) are shown in Fig. 3. The curves are shifted
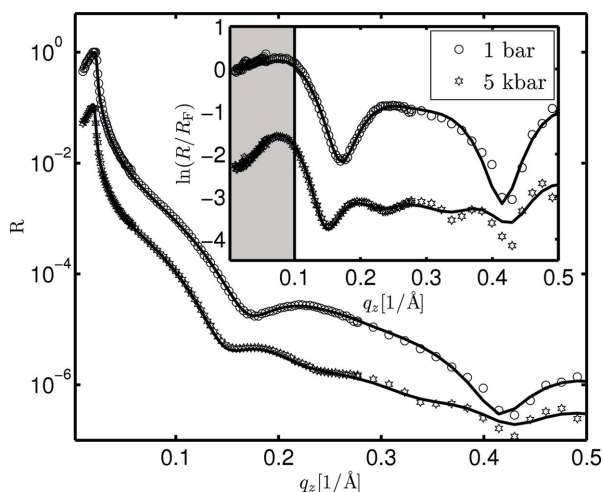
**Figure 3**
Reflected intensity *versus* wavevector transfer $q_z$ at 1 bar (circles) and 5 kbar (stars). Solid lines are fits to the data. The inset shows the same data, but normalized to the Fresnel reflectivity $R_F$. The gray area indicates the $q_z$-range covered by the neutron study of Koo *et al.* (2013).



**Figure 4**
Normalized electron density *versus* distance over the sample *z*. The solid (blue) line corresponds to 1 bar and the (red) dotted line to 5 kbar. The (black) dot-dashed line is the 1 bar profile after substraction of the protein layer.

vertically for better visibility. Solid lines correspond to fits to the data. The X-ray reflectivity data were refined using the Parratt algorithm (Parratt, 1954) in combination with the effective density model. The Parratt algorithm is based on a recursive determination of the reflected and transmitted intensity at each interface in the system. The effective density model is useful when the layer roughness is of the same order of magnitude as the layer thickness, that is, in a regime where the traditional approach of distinct slabs fails (Tolan, 1999). Also, a footprint correction was applied to the data to account for the finite sample size.

## 4. Discussion

From Fig. 3, significant changes in the reflectivity curves can be observed. These changes are emphasized by a normalization to the Fresnel reflectivity of an ideally flat silicon surface, as presented in the inset of the figure.

For a detailed understanding of the interfacial structure, we analyze the electron density profiles that can be obtained from the refinements in Fig. 3, using the entire $q_z$-range up to 0.5 Å$^{-1}$. The gray region in the inset shows the limited $q_z$-range that is accessible by high-pressure neutron reflectivity measurements. The interpretation of experimental data acquired during lysozyme adsorption at solid/liquid interfaces might become highly ambiguous if the $q_z$-range is too small.

The electron density profiles that we obtained from the XRR data are shown in Fig. 4. They are normalized to the electron density of the silicon substrate and are shown as a function of *z*. The solid (blue) line corresponds to 1 bar and the (red) dashed line to 5 kbar. The (black) dot-dashed line is the 1 bar profile after substraction of the protein layer.

The silicon wafer is modeled by the bulk silicon and a silicon dioxide layer, the thickness of which depends on the wafer cleaning procedure. At the bottom of the figure, a simple box model sketches the substrate. Directly adjacent to the silicon
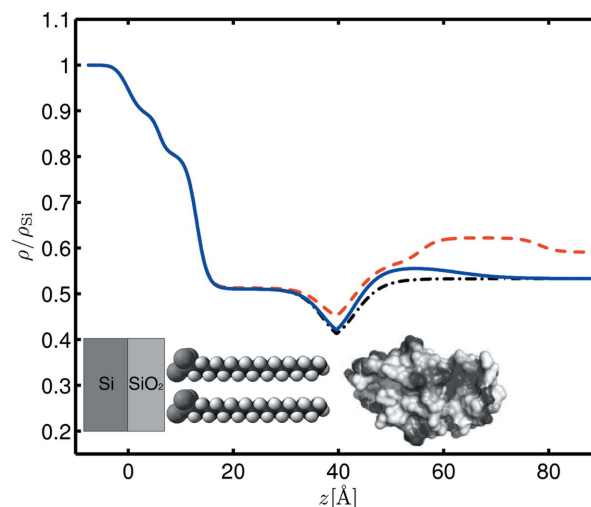
dioxide is the hydrophobic OTS film, modeled by two layers, representing the molecule head and tail groups. We obtained a thickness of ∼6 Å for the head group and ∼24 Å for the tail group. This is in good agreement with the results of other researchers. Mezger *et al.* (2006) determined in their studies a head group size of ∼5.7 Å and a tail length of 21.8 Å. The theoretical length of the unstretched chain can be estimated from the C—C bond length to be ∼23 Å, which lies within our experimental resolution. Thus, we conclude that the OTS chains on our sample are not or only slightly tilted.

Above 80 Å lies the liquid bulk phase. It is not pure water, but a mixture of water, lysozyme and salt. This given, the value of roughly half the density of silicon is in good agreement with the theoretical bulk water level of 0.47 times the electron density of silicon (NIST, http://webbook.nist.gov/chemistry/). The bulk electron density of pure water is in theory increased by 13% if the pressure is increased from 1 bar and 5 kbar (NIST). The increase of electron density is caused by the compression of the bulk water phase. Given that salt has an effect on the compressibility of water, the increase of 11% in our experiments is in the expected range.

The dip in the electron density adjacent to the OTS tail groups, around *z* = 40 Å, is striking. It corresponds to the so-called hydrophobic gap, an electron-density-depleted region that was earlier observed between hydrophobic surfaces and water and was investigated in several experimental and numerical studies (Poynor *et al.*, 2006; Mezger *et al.*, 2006, 2010; Maccarini *et al.*, 2007; Chattopadhyay *et al.*, 2010). Its structural interpretation is still under discussion.

From our experiments, we observe the adsorption of a lysozyme layer onto the OTS layer (see the increase in the electron density in Fig. 4 above ∼40 Å). It is natural to assume that the protein layer does not hover over the OTS layer, but that it is adsorbed to it. However, we still observe an electron-depleted region close to the OTS tails. Thus, we argue that the protein is oriented towards the hydrophobic OTS with its

hydrophobic side chains with many protons and few electrons, leading to an effective reduced electron density. At ambient pressure, this effect was also observed by Hähl *et al.* (2012) and Richter & Kuzmenko (2013).

In Fig. 4, the solid (blue) line corresponds to a measurement at 1 bar. The dot-dashed (black) line represents the same 1 bar profile after substraction of the electron density of the protein layer. A comparison between the two curves in the region above the OTS layer allows more to be learned about the protein adsorption. At 1 bar, the deviation between the two curves starts in the region of depleted electron density around 40 Å and extends up to around 75 Å. This 35 Å layer corresponds to a monolayer of lysozyme. Protein monolayer adsorption under similar conditions was observed previously (Hähl *et al.*, 2012; Richter & Kuzmenko, 2013; Evers *et al.*, 2008) and is known to be stable in time. We added a simple graphical model to the electron density profile, illustrating this most probable scenario that we can extract from the experiments.

If the pressure is increased to 5 kbar, a region of even higher electron density appears and extends from 40 Å to 80 Å, most pronounced between 60 Å and 80 Å. As this hump has clearly a higher electron density than the lysozyme layer at 1 bar, it is certain that a more densely packed protein layer is accumulating at the interface. However, we cannot give more details about the exact shape of the protein in this extra layer. We conclude that high hydrostatic pressure has a significant impact on the adsorption behavior of proteins at hydrophobic interfaces.

## 5. Conclusion

We report on the first X-ray reflectivity measurements of the solid/liquid interface at high hydrostatic pressures up to 5 kbar. To perform X-ray reflectivity measurements at such high pressures, a new sample environment was designed, consisting of an outer highly pressure-resisting cell and an inner sample cell. The inner cell can compensate for volume changes caused by the increased pressure and also protects the solid substrate against a shift in the position, which is crucial for XRR measurements. The cell is optimized for high photon energies ≥ 20 keV and can accept beams with a height of up to 0.1 mm. At 5 kbar, the pressure stability is ±1%. The temperature can be varied between 274 K and 360 K and kept constant with a stability of 0.1 K.

In first measurements, we demonstrated the pressure-induced adsorption of lysozyme at a hydrophobic solid substrate in the presence of a chaotropic co-solvent. An increase of the layer thickness beyond monolayer formation, as is the case at ambient pressure, was observed at 5 kbar, since lysozyme adsorbs at the interface triggered by pressure. We also showed that the size of the hydrophobic gap changes only slightly with increasing pressure. This phenomenon will be interesting to study in the future, and will increase the understanding of how the water structure influences the structure of solid/liquid interfaces.

## References

Als-Nielsen, J. & McMorrow, D. (2001). *Elements of Modern X-ray Physics.* New York: John Wiley and Sons.

Ando, N., Chenevier, P., Novak, M., Tate, M. W. & Gruner, S. M. (2008). *J. Appl. Cryst.* **41**, 167–175.

Boewer, L., Nase, J., Paulus, M., Lehmkühler, F., Tiemeyer, S., Holz, S., Pontoni, D. & Tolan, M. (2012). *J. Phys. Chem. C*, **116**, 8548.

Carmichael, J. R., Rother, G., Browning, J. F., Ankner, J. F., Banuelos, J. L., Anovitz, L. M., Wesolowski, D. J. & Cole, D. R. (2012). *Rev. Sci. Instrum.* **83**, 045108.

Chattopadhyay, S., Uysal, A., Stripe, B., Ha, H. Y., Marks, T. J., Karapetrova, E. A. & Dutta, P. (2010). *Phys. Rev. Lett.* **105**, 037803.

Evers, F., Shokuie, K., Paulus, M., Sternemann, C., Czeslik, C. & Tolan, M. (2008). *Langmuir*, **24**, 10216–10221.

Hähl, H., Evers, F., Grandthyll, S., Paulus, M., Sternemann, C., Loskill, P., Lessel, M., Hüsecken, A. K., Brenner, T., Tolan, M. & Jacobs, K. (2012). *Langmuir*, **28**, 7747–7756.

Hong, X., Newville, M. & Duffy, T. S. (2013). *J. Phys. Conf. Ser.* **430**, 012120.

Ingalls, R., Crozier, E. D., Whitmore, J. E., Seary, A. J. & Tranquada, J. M. (1980). *J. Appl. Phys.* **51**, 3158.

Ishimatsu, N., Matsumoto, K., Maruyama, H., Kawamura, N., Mizumaki, M., Sumiya, H. & Irifune, T. (2012). *J. Synchrotron Rad.* **19**, 768–772.

Jackler, G., Steitz, R. & Czeslik, C. (2002). *Langmuir*, **18**, 6565–6570.

Jackson, M. J., Sturhahn, W., Shen, G., Zhao, J., Hu, M. Y., Errandonea, D., Bass, J. D. & Fei, Y. (2005). *Am. Mineral.* **90**, 199–205.

Jayaraman, A. (1983). *Rev. Mod. Phys.* **55**, 65.

Jeworrek, C., Steitz, R., Czeslik, C. & Winter, R. (2011). *Rev. Sci. Instrum.* **82**, 025106.

Kato, M. & Fujisawa, T. (1998). *J. Synchrotron Rad.* **5**, 1282–1286.

Katrusiak, A. & McMillan, P. (2004). Editors. *High Pressure Crystallography.* Dordrecht: Kluwer.

Koo, J., Erlkamp, M., Grobelny, S., Steitz, R. & Czeslik, C. (2013). *Langmuir*, **29**, 8025–8030.

Kreuzer, M., Kaltofen, T., Steitz, R., Zehnder, B. H. & Dahint, R. (2011). *Rev. Sci. Instrum.* **82**, 023902.

Krywka, C., Paulus, M., Sternemann, C., Volmer, M., Remhof, A., Nowak, G., Nefedov, A., Pöter, B., Spiegel, M. & Tolan, M. (2006). *J. Synchrotron Rad.* **13**, 8–13.

Krywka, C., Sternemann, C., Paulus, M., Javid, N., Winter, R., Al-Sawalmih, A., Yi, S., Raabe, D. & Tolan, M. (2007). *J. Synchrotron Rad.* **14**, 244–251.

Krywka, C., Sternemann, C., Paulus, M., Tolan, M., Royer, C. & Winter, R. (2008). *ChemPhysChem*, **9**, 2809–2815.

Lehmkühler, F., Paulus, M., Sternemann, C., Lietz, D., Venturini, F., Gutt, C. & Tolan, M. (2009). *J. Am. Chem. Soc.* **131**, 585–589.

Liu, Y., Spring, J. D., Steinhart, M. & Bansil, R. (2012). *Macromolecules*, **45**, 9147–9154.

Loubeyre, P., LeToullec, R., Hausermann, D., Hanfland, M., Hemley, R. J., Mao, H. K. & Finger, L. W. (1996). *Nature (London)*, **383**, 702–704.

McCammon, C., Kantor, I., Narygina, O., Rouquette, J., Ponkratz, U., Sergueev, I., Mezour, M., Prakapenka, V. & Dubrovinsky, L. (2008). *Nat. Geosci.* **1**, 684–687.

Maccarini, M., Steitz, R., Himmelhaus, M., Fick, J., Tatur, S., Wolff, M., Grunze, M., Janecek, J. & Netz, R. R. (2007). *Langmuir*, **23**, 598–608.

McMahon, M. I. (2012). *Advanced X-ray Crystallography*, edited by K. Rissanen, *Topics in Current Chemistry*, Vol. 315, pp. 69–110. Berlin: Springer.

Meade, C., Hemley, R. J. & Mao, H. K. (1992). *Phys. Rev. Lett.* **69**, 1387–1390.

Mezger, M., Reichert, H., Schöder, S., Okasinski, J., Schröder, H., Dosch, H., Palms, D., Ralston, J. & Honkimäki, V. (2006). *Proc. Natl Acad. Sci. USA*, **103**, 18401–18404.

Mezger, M., Sedlmeier, F., Horinek, D., Reichert, H., Pontoni, D. & Dosch, H. (2010). *J. Am. Chem. Soc.* **132**, 6735–6741.

Neuman, R. C., Kauzmann, W. & Zipp, A. (1973). *J. Phys. Chem.* **77**, 2687–2691.

Parratt, L. G. (1954). *Phys. Rev.* **95**, 359–369.

Paulus, M., Lietz, D., Sternemann, C., Shokuie, K., Evers, F., Tolan, M., Czeslik, C. & Winter, R. (2008). *J. Synchrotron Rad.* **15**, 600–605.

Poynor, A., Hong, L., Robinson, I. K., Granick, S., Zhang, Z. & Fenter, P. A. (2006). *Phys. Rev. Let.* **97**, 266101.

Pressl, K., Kriechbaum, M., Steinhart, M. & Laggner, P. (1997). *Rev. Sci. Instrum.* **68**, 4588.

Richter, A. G. & Kuzmenko, I. (2013). *Langmuir*, **29**, 5167–5180.

Rueff, J. P. & Shukla, A. (2010). *Rev. Mod. Phys.* **82**, 847–896.

Schellman, J. A. (2002). *Biophys. Chem.* **96**, 91–101.

Schroer, M. A., Markgraf, J., Wieland, D. C., Sahle, C. J., Möller, J., Paulus, M., Tolan, M. & Winter, R. (2011). *Phys. Rev. Lett.* **106**, 178102.

Tateno, S., Hirose, K., Ohishi, Y. & Tatsumi, Y. (2010). *Science*, **330**, 359–361.

Tolan, M. (1999). *X-ray Scattering from Soft Matter Thin Films, Springer Tracts in Modern Physics*, Vol. 148. Berlin: Springer.

Tolan, M., Weis, T., Westphal, C. & Wille, K. (2003). *Synchrotron Radiat. News*, **16**, 9–11.

Venturini, F., Schöder, S., Kuhs, W. F., Honkimäki, V., Melesi, L., Reichert, H., Schober, H. & Thomas, F. (2011). *J. Synchrotron Rad.* **18**, 251–256.

Wang, P., Lerner, A. H., Taylor, M., Baldwin, J. K., Grubbs, R. K., Majewski, J. & Hickmott, D. D. (2012). *Eur. Phys. J. Plus*, **127**, 76.

Winter, R. (2002). *Biochim. Biophys. Acta*, **1595**, 160–184.

Woenckhaus, J., Köhling, R., Winter, R., Thiyagarajan, P. & Finet, S. (2000). *Rev. Sci. Instrum.* **71**, 3895.